Further result on the zeros of a rigid-flexible link manipulator

M. Vakil, R. Fotouhi, P. N. Nikiforuk

Mechanical Engineering Department, University of Saskatchewan,

m.vakil, reza.fotouhi, peter.nikiforuk@usask.ca

Abstract

Because of the nonminimum phase characteristics, the end-effector trajectory tracking of flexible link manipulators is a challenging problem. The nonminimum phase feature means that, for a linearized model, the transfer function between the end-effector displacement and the base torque has right-hand-side zeros. The locations of these zeros influence the performance of the end-effector controllers, which is a novelty of this research work. In this paper a study of the zeros of the transfer function is performed. It is shown that there are physical parameters where the increase in their values moves the zeros further from the imaginary axis; while by increasing the values of some other physical parameters the zeros move closer to the imaginary axis. Finally, there are physical parameters where the location of the zeros are independent of their values.

Key word: transfer function, end-effector control, flexible link manipulator

1. INTRODUCTION

The nonminimum characteristics of flexible link manipulators have turned their end-effector control into a challenging problem [1]. For a slewing single flexible link manipulator, shown in Fig. 1, the nonminimum phase feature means that the transfer function, between the base torque τ and the end-effector displacement *y*, has right-hand-side (RHS) zeros in domain S of the Laplace transform.

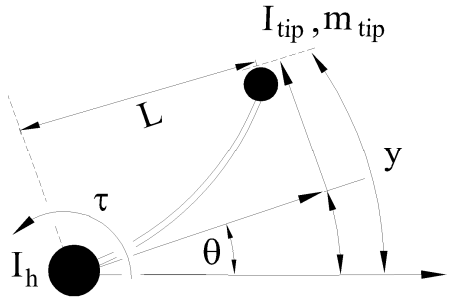

Fig. 1: Schematic of a slewing single flexible link manipulator

The nonminimum phase characteristic creates several challenges in the design of end-effector trajectory-tracking controllers; some of these are (*i*)- Non-causal end-effector inverse dynamic calculation [2] and (*ii*)- the dependency of the performance of the end-effector controllers on the location of RHS zeros [3, 4 page 265, 5,6,7,8]. Thus

the study of the zeros and the change in their locations due to the changes in the physical parameters are of great importance, which has been investigated in this paper. For this purpose, a single flexible link manipulator with the initial part of the link being rigid, as shown in Fig. 2a, is considered [9]. This manipulator is referred to as a slewing single rigid-flexible link manipulator (SRFLM). The reasons for introducing and studying the zeros of a SRFLM is that the precise modeling of an experimental single flexible link manipulator, like the one shown in Fig. 2b, requires that it be treated as a SRFLM. The initial rigid portion for this manipulator is due to the mounting brackets.

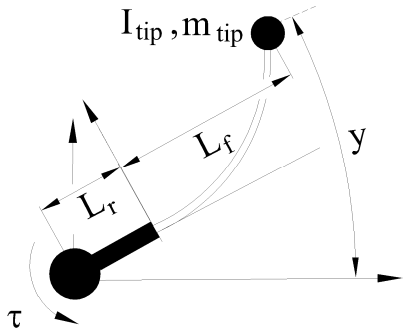

Fig. 2a: The schematic of a SRFLM

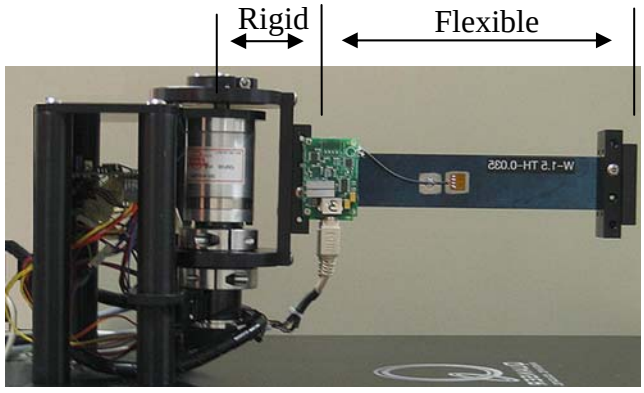

Fig. 2b: Flexible manipulator available in the Robotics Laboratory of the University of Saskatchewan

After introducing SRFLM, the zeros of a SRFLM[1] are found based on authors' new theorem [10] which does not need deriving the corresponding transfer function. This theorem states that:

Theorem: *The zeros of the transfer function of a slewing single rigid-flexible link manipulator {SRFLM}, considering the torque at the base as the input and the*

[1] In the rest of this paper, the words "zeros of SRFLM" refer to the zeros of the transfer function of a SRFLM considering the base torque as the input and end-effector displacement as the output.

manipulator {SRFLM}, considering the torque at the base as the input and the displacement of the end-effector as the output, are the same as the zeros of the transfer function of the pinned-pinned counterpart of the SRFLM, considering the torque at the base as the input and the shear force at the end-effector (other end) as the output.

That is, the zeros of the transfer function $G = Y(s)/\tau(s)$ in Fig. 2a are the same as the zeros of the transfer function $F = \upsilon(s)/\tau(s)$ in Fig. 3; υ is the end-effector shear force.

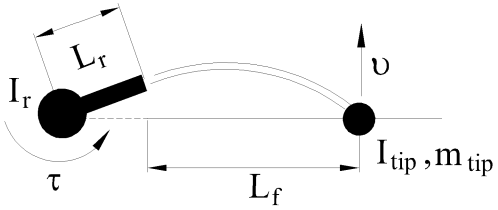

Fig. 3: The pinned-pinned counterpart of a SRFLM which is shown in Fig. 2a

After having the location of the zeros, the change in the location of the zeros due to the changes in all the physical parameters is studied. It was shown that the change in the mass of the payload and mass moment of inertia of the rigid section do not change the location of the zeros. However by increasing (or decreasing) the rigidity of the flexible section and the mass moment of inertia of the payload, the zeros move further from (or get closer to) the imaginary axis. Moreover by increasing (or decreasing) the mass per unit length of the flexible section and the lengths of the rigid and flexible sections, the zeros get closer to (or move further from) the imaginary axis.

2. ZEROS OF A SINGLE RIGID-FLEXIBLE LINK MANIPULATOR

In this paper the zeros of the SRFLM will be calculated by adopting the theorem given in Section introduction. That is, the SRFLM is first pinned at the end-effector as shown in Fig. 4, and then the zeros of the pinned-pinned counterpart of the SRFLM, between the base torque and end-effector shear force, are obtained.

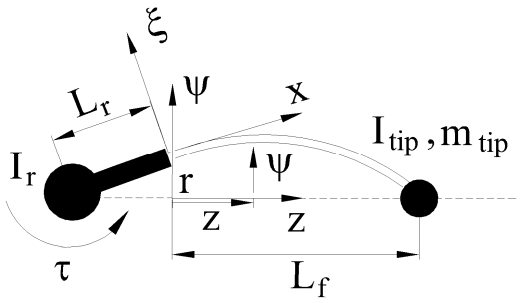

Fig. 4: Pinned-pinned counterpart of a SRFLM which is shown in Fig. 2a

The dynamic equation for the flexible portion of the SRFLM is:

$$\rho\psi_{tt}(z,t) + EI\psi_{zzzz}(z,t) = 0 \tag{1}$$

where z and ψ are measured from point *r* as shown in Fig. 4. Moreover, ρ is the mass per unit length of the flexible section, EI is the rigidity of the flexible section and $\psi_t(x,t)$ and $\psi_x(x,t)$ are the partial derivatives of $\psi(x,t)$ with respect to t and x, respectively, and a similar notation adopted for higher derivatives. Moreover, the associated boundary conditions for the pinned-pinned counterpart of the SRFLM are:

$$\psi(0,t) = L_r\,\psi_z(0,t) \tag{2a}$$

$$\psi(L_f,t) = 0 \tag{2b}$$

$$\tau + EI\psi_{zz}(0,t) - L_r EI\psi_{zzz}(0,t) = I_r\psi_{ztt}(0,t) \tag{2c}$$

$$EI\psi_{zz}(L_f,t) + I_{tip}\psi_{ztt}(L_f,t) = 0 \tag{2d}$$

where I_r is the mass moment of inertia of the rigid section with respect to the base, m_{tip} and I_{tip} are the mass and mass moment of inertia of the payload, L_f is the length of the flexible section and L_r is the length of the rigid section. Eq. (2a) is due to the fact that the flexible section is clamped to the rigid section. Eq. (2b), shows that the flexible section is pinned at the end-effector. Eqs. (2c) and (2d) represent the momentum balance for the rigid section and the payload, respectively.

Taking the Laplace transform of Eq. (1) leads to:

$$\frac{d^4\psi(z,s)}{dz^4} - \lambda^4\psi(z,s) = 0 \tag{3}$$

where:

$$\lambda^4 = -\frac{\rho\, s^2}{EI} \tag{4}$$

and $\psi(z,s)$ is the Laplace transform of $\psi(z,t)$. From Eq. (3):

$$\psi(z,s) = c_1\cos(\lambda z) + c_2\sin(\lambda z) + c_3\cosh(\lambda z) + c_4\sinh(\lambda z) \tag{5}$$

and the unknown c_1, c_2, c_3 and c_4 are found by imposing the boundary conditions presented in Eqs. (2a -2d). Having $\psi(z,s)$ and also knowing that the shear force at the end-effector is $\upsilon(L_f,s) = EI\psi_{zzz}(L_f,s)$, the transfer function of the pinned-pinned counterpart of the SRFLM is:

$$F(s) = \frac{EI\psi_{zzz}(L_f, s)}{\tau(s)} = \frac{N_F(s)}{D_F(s)} \tag{6}$$

where $N_F(s)$ and $D_F(s)$ are the numerator and denominator of the transfer function $F(s)$.

To find the zeros of $F(s)$ which are the zeros of a SRFLM (between the base torque and end-effector displacement), the condition $N_F(s) = 0$ has to be imposed, which results in:

$$\begin{aligned} &\left[\sin(\lambda L_f) + \sinh(\lambda L_f) + \lambda^3(\frac{I_{tip}}{\rho})(\cos(\lambda L_f) - \cosh(\lambda L_f))\right] + \\ &L_r\left[\lambda(\cos(\lambda L_f) + \cosh(\lambda L_f)) - \lambda^4(\frac{I_{tip}}{\rho})(\sin(\lambda L_f) + \sinh(\lambda L_f))\right] = 0 \end{aligned} \tag{7}$$

By assuming $\beta = \lambda L_f$, Eqs. (4) and (7) are respectively :

$$s^2 = -\beta^4 \frac{EI}{\rho L_f{}^4} \tag{8}$$

$$\begin{aligned} &\left[\sin(\beta) + \sinh(\beta) + \beta^3(\frac{I_{tip}}{3I_{rb}})(\cos(\beta) - \cosh(\beta))\right] + \\ &\frac{L_r}{L_f}\left[\beta(\cos(\beta) + \cosh(\beta)) - \beta^4(\frac{I_{tip}}{3I_{rb}})(\sin(\beta) + \sinh(\beta))\right] = 0 \end{aligned} \tag{9}$$

where $I_{rb} = \rho L_f^3 / 3$. Thus the zeros of a SRFLM, that is the values of *s*, are obtained from Eq. (8) where β are the roots of Eq. (9). Since SRFLM has infinite modes of vibration and for each mode of vibration there is a pair of zeros, the zeros of a SRFLM are infinite. Thus, for a given L_r / L_f and I_{tip} / I_{rb}, Eq. (9) results in an infinite number of β values.

Remark 1: The zeros of a SRFLM were also obtained by deriving the transfer function $G = Y(s)/\tau(s)$ of Fig. 2a and were exactly the same as those obtained from Eqs. (8) and (9). This comparison was a check to verify the authors' new theorem.

3. RESULTS AND DISCUSSIONS:

The roots of Eq. (9) depend on the ratios I_{tip} / I_{rb} and L_r / L_f. To investigate the effect of these ratios on the location of the zeros, Eq. (9) has to be solved numerically. To solve this equation, a nonlinear solver was written in MATLAB.

In Figs. 5 variation of the zeros for the first mode of vibration versus I_{tip}/I_{rb} and L_r/L_f is shown.

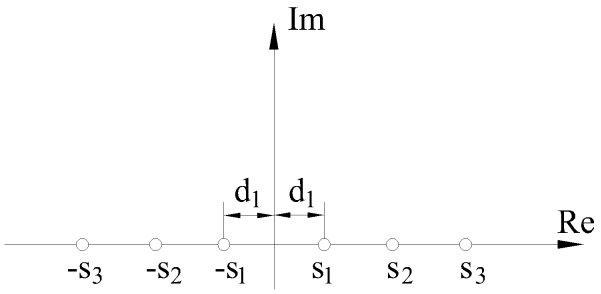

Fig. 5a: Schematic of the zeros of the first vibration mode, $(-s_1, s_1)$

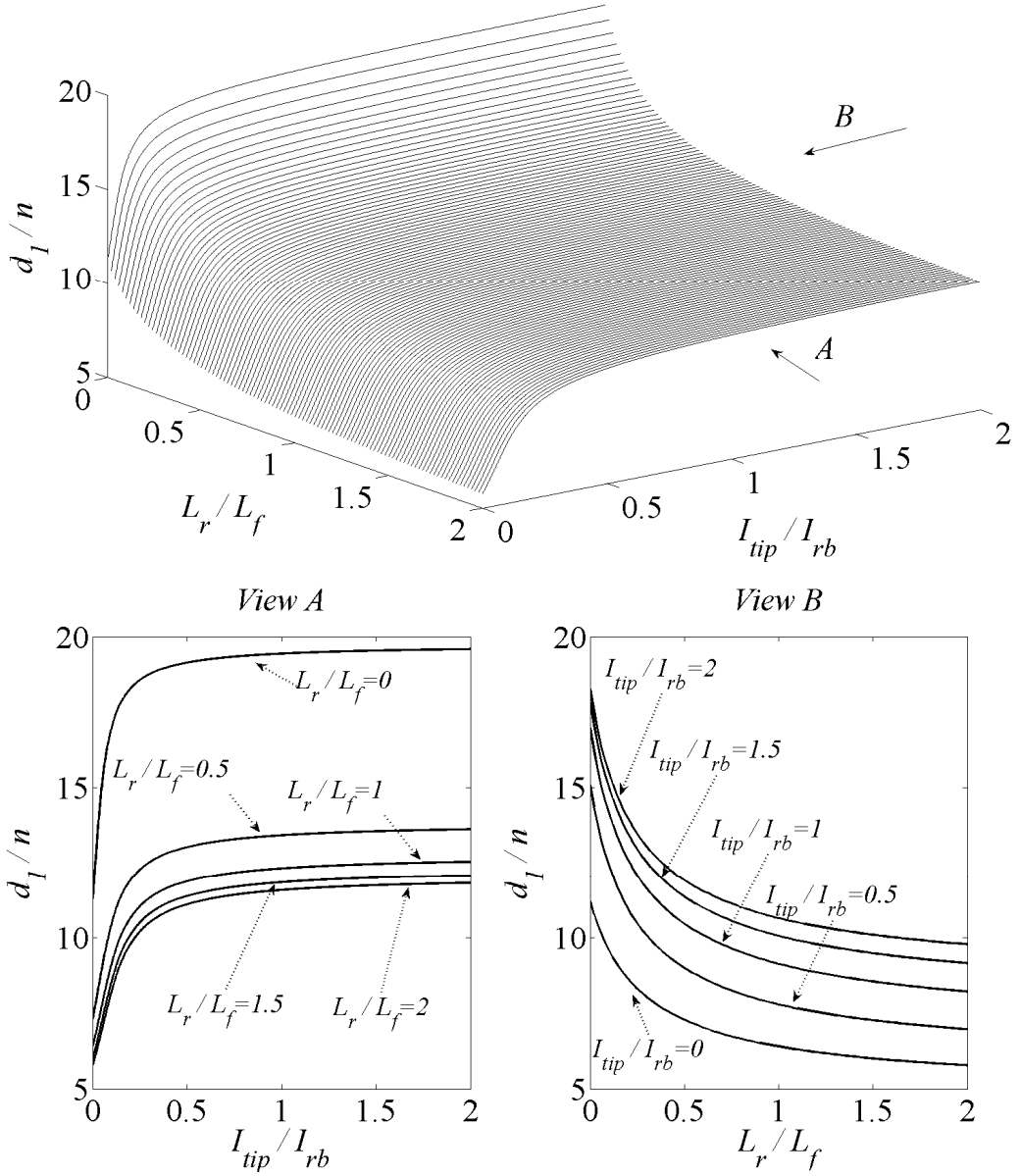

Fig. 5b: Variation of d_1 in Fig. 5a versus I_{tip}/I_{rb} and L_r/L_f ($n=\sqrt{EI/\rho L_f^4}$, $I_{rb}=\rho L_f^3/3$)

Similar trends as that in Fig. 5 exist for the zeros associated with higher modes of vibration which are not presented here due to space limitations. From Eqs. (8) and (9) and Figs. 5 the following conclusions are drawn:

1- The rigidity of the flexible portion, EI, does not affect the values of β in Eq. (9). However, the factor $EI/\rho L_f^4$ in Eq. (8) (n in Fig. 5b) represents the change in the zeros' locations because of the change in the rigidity. Also by increasing (or decreasing) the rigidity of the flexible section, while all other physical parameters are constant, the zeros move further from (or get closer to) the imaginary axis.

2- The location of the zeros for a SRFLM will not directly be changed by the value of the mass of the payload m_{tip}. This is due to the fact that m_{tip} did not appear in Eqs. (8) and (9) which determine the location of the zeros. However, the zeros dependents on the mass moment of inertia of the payload I_{tip}. This independence of the zeros to the mass of the payload m_{tip} agrees with the physical interpretation of the zeros given in [11] and has also been mentioned in [12] for a SFLM.

3- From view A in Figs. 5b, it is clear that the larger (or smaller) I_{tip}, the further from (or the closer to) the imaginary axis the zeros are, assuming all other physical parameters are constant. However, there is a saturation limit for how far (or close) the zeros will move away (get close to) the imaginary axis by increasing (or decreasing) I_{tip}.

4- The location of the zeros of a SRFLM does not depend on the mass moment of inertia of the rigid portion I_r. This is due to the fact that I_r did not appear in Eqs. (8) and (9) which determine the location of the zeros. For the SFLM of Fig. 1 this means that the location of the zeros does not depend on the mass moment of inertia of hub I_h.

5- From View B in Figs. 5b, it is clear that the larger (or smaller) L_r, the closer to (the further from) the imaginary axis the zeros are.

6- The larger (or smaller) L_f, the closer to (the further from) the imaginary axis the zeros are. It is to be noted that this conclusion cannot be drawn from Fig. 5 since by changing L_f, all ratios L_r/L_f, $n=\sqrt{EI/\rho L_f^4}$ and I_{tip}/I_{rb} will change. However, the variation of the zeros of the first mode shape of a SRFLM, shown in Fig. 6 versus L_f/L_r, clearly indicates this conclusion. In Fig. 6 by changing L_f only the ratio L_f/L_r will be

changed. To draw Fig. 6, Eqs. (8) and (9) were rearranged and solved as detailed in Appendix I.

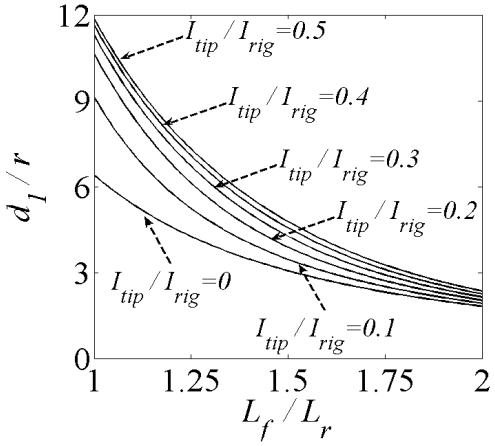

Fig. 6: Variation of d_1 versus L_f / L_r ($r = \sqrt{EI / \rho L_r^4}, I_{rig} = \rho L_r^3 / 3$)

7- The larger (or smaller) the mass per unit length of the link ρ, the closer to (or the further from) the imaginary axis the zeros are. This conclusion can easily be drawn from Fig. 7. This figure was obtained from Figs. 5b with the details provided in Appendix II.

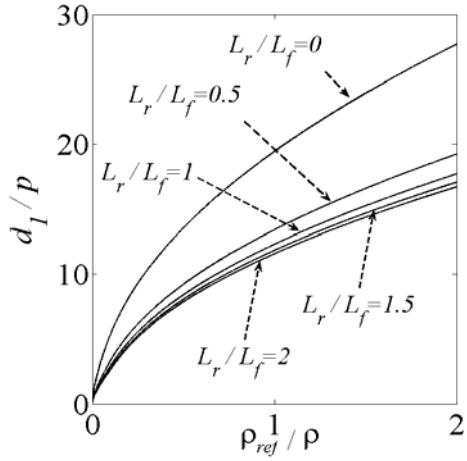

Fig. 7: Variation of d_1 versus ρ ($p = \sqrt{EI / 3I_{tip}L_f}, \rho_{ref} = 3I_{tip} / L_f^3$

4. CONCLUSIONS

A slewing single rigid-flexible link manipulator (SRFLM) is considered. For the first time, it was shown that the physical parameters of a SRFLM fall into three categories with regard to changing the location of the zeros, which is the main contribution of this work. The first category was composed of the mass moment of inertia of the rigid section and the mass of the payload. In this category no change in the location of zeros will occur by changing these physical parameters. The second category

was composed of the mass moment of inertia of the payload and the rigidity of the flexible portion, whereby increasing (or decreasing) these physical parameters the zeros move further from (or get closer to) the imaginary axis. The third category are the physical parameters, whereby increasing (or decreasing) their values the zeros get closer to (or move further from) the imaginary axis. These physical parameters are mass per unit length of the flexible section and the lengths of the rigid and flexible sections. Finally it was observed that there is a limit for how far (or how close) the zeros can move away (or get close) to the imaginary axis by increasing (or decreasing) the mass moment of inertia of the payload, while all other physical parameters are constant.

REFERENCES

1. F. Y. Wang, and Y. Gao, *Advanced Studies of Flexible Robotic Manipulators: Modeling, Design, Control and Applications* (World Scientific, New Jersey, USA, 2003).

2. B. Paden, D. Chen, R. Ledesma and E. Bayo, Exponentially Stable Tracking Control for Multi-Joint Flexible-Link Manipulators, ASME Journal of Dynamic Systems, Measurement and Control, Vol. 115, pp. 53-59, March 1993.

3. S. Devasia, Approximated Stable Inversion for Nonlinear System with Nonhyperbolic Internal Dynamics, *IEEE Transactions on Automatic Control*, 44(7), 1419-1425, 1999.

4. J. J. Slotine and W. Li, *Applied Nonlinear Control*, Prentice Hall, NJ, USA, 1991.

5. X. Wang and D. Chen, Output Tracking Control of a One-Link Flexible Manipulator via Causal Inversion, *IEEE Transactions on Control System Technology*, 14 (1), 141-148, 2006.

6. Y. Feng, B. Bao and X. Yu, Inverse dynamics nonsingular terminal sliding mode control of two-link flexible manipulator, *International Journal of Robotics and Automations*, 19 (2), 2004, 91-102.

7. M. Moallem, R. V. Patel and K. Khorasani, *Flexible-link robot manipulators, Control techniques and Structural design*, 2000, London, Springer.

8. H. S. Park, P. H. Chang and D. Y. Lee, Trajectory planning for the tracking control of systems with unstable zeros, *Mechatronics*, 13, 2003, 127-139

9. M. Vakil, R. Fotouhi, P. N. Nikiforuk, Zeros of the trasnfer function of a rigid-flexible manipulator, *the 21st Canadian Congress of Applied Mechanics, Toronto, Ontario, Canada*, Paper No. GP_75 (CD Rom), 2007.

10. M. Vakil, R. Fotouhi, P. N. Nikiforuk, On the zeros of the transfer function of a single flexible link manipulator, *17th IASTED International conference on Modeling and Simulation, Montreal, Quebec, Canada*, 2006, 20-25.

11. D.K. Miu, Physical Interpretation of Transfer Function Zeros for Simple Control Systems with Mechanical Flexibility, *Journal of Dynamic Systems, Measurement and Control,* 13(3), 419-424, 1991.

12. V.A. Spector and H. Flashner, Modeling and Design Implications of Noncollocated Control in Flexible Systems, *Journal of Dynamic Systems, Measurement and Control*, 112(2), 186-193, 1990.

APPENDIX I: REARRANGING EQS. (8) AND (9) TO OBTAIN FIG. 6

The variable δ is defined as:

$$\delta = \lambda L_r \tag{A1}$$

Therefore, form (A1):

$$\lambda = \frac{\delta}{L_r} \tag{A2}$$

Substituting λ From Eq. (A2) in Eqs. (8) results in:

$$s^2 = -\delta^4 \frac{EI}{\rho L_r^{\,4}} \tag{A3}$$

Moreover substituting λ From Eq. (A2) in Eq. (9) leads to:

$$\begin{aligned} &\left[\sin(\delta\frac{L_f}{L_r}) + \sinh(\delta\frac{L_f}{L_r}) + \delta^3(\frac{I_{tip}}{3I_{rig}})(\cos(\delta\frac{L_f}{L_r}) - \cosh(\delta\frac{L_f}{L_r}))\right] + \\ &\left[\delta(\cos(\delta\frac{L_f}{L_r}) + \cosh(\delta\frac{L_f}{L_r})) - \delta^4(\frac{I_{tip}}{3I_{rig}})(\sin(\delta\frac{L_f}{L_r}) + \sinh(\delta\frac{L_f}{L_r}))\right] = 0 \end{aligned} \tag{A4}$$

where $I_{rig} = \rho L_r^3 / 3$. Therefore, the zeros of a SRFLM, the values of *s*, can be obtained from Eq. (A3) where δ has to be found by solving Eq. (A4).

To obtain Fig. 6, Eq. (A4) was first solved for δ versus L_f / L_r and assuming that I_{tip} / I_{rig} is constant. Then the obtained values of δ were substituted into Eq. (A3) and plotted versus L_f / L_r.

APPENDIX II: OBTAINING FIG. 7 FROM FIG. 5b

In Figs 7, the graphical relation between d / n versus I_{tip} / I_{rb} and L_r / L_f is

presented. This graphical relation can be represented as:

$$\frac{d_1}{n} = \Lambda_1\left(\frac{L_r}{L_f}, \frac{I_{tip}}{I_{rb}}\right) \tag{A5}$$

where Λ_1 is the functions which is schematically shown in Fig. 5b. Multiplying both side of Eq. (A5) with $\sqrt{I_{tip} / I_{rb}}$ yield to:

$$\sqrt{\frac{I_{tip}}{I_{rb}}}\frac{d_1}{n} = \sqrt{\frac{I_{tip}}{I_{rb}}}\Lambda_1\left(\frac{L_r}{L_f}, \frac{I_{tip}}{I_{rb}}\right) \tag{A6}$$

By using the definition of $n = \sqrt{EI / \rho L_f^4}$ and $I_{rb} = \rho L_f^3 / 3$, the left hand side of Eq. (A6) changes to:

$$\sqrt{\frac{I_{tip}}{I_{rb}}}\frac{d_1}{n} = \frac{d_1}{p} \tag{A7}$$

where $p = \sqrt{EI / 3 I_{tip} L_f}$. Moreover, by using the definition $I_{rb} = \rho L_f^3 / 3$, the ratio $\frac{I_{tip}}{I_{rb}}$ is:

$$\frac{I_{tip}}{I_{rb}} = \frac{\rho_{ref}}{\rho} \tag{A8}$$

where $\rho_{ref} = 3 I_{tip} / L_f^3$. Combining Eqs. (A6), A(7) and (A8) results in:

$$\frac{d_i}{p} = \sqrt{\frac{\rho_{ref}}{\rho}}\Lambda_1\left(\frac{L_r}{L_f}, \frac{\rho_{ref}}{\rho}\right) \tag{A9}$$

For different constant values of L_r / L_f, the variation of Λ_i versus ρ_{ref} / ρ is given in View A of Fig. 5b (Note that from Eq. (A8) $I_{tip} / I_{rb} = \rho_{ref} / \rho$). By multiplying the values of Λ_1 at each ρ_{ref} / ρ (given in View A of Fig. 5b) with $\sqrt{\rho_{ref} / \rho}$ the right hand side of Eq. (A9) was obtained. Consequently d_1 / p, left hand side of Eq. (A9), could be plotted versus ρ_{ref} / ρ as presented in Fig. 7.